iScience

CellPress
OPEN ACCESS

Article

Long noncoding RNA LINC01435 impedes diabetic wound healing by facilitating YY1-mediated HDAC8 expression

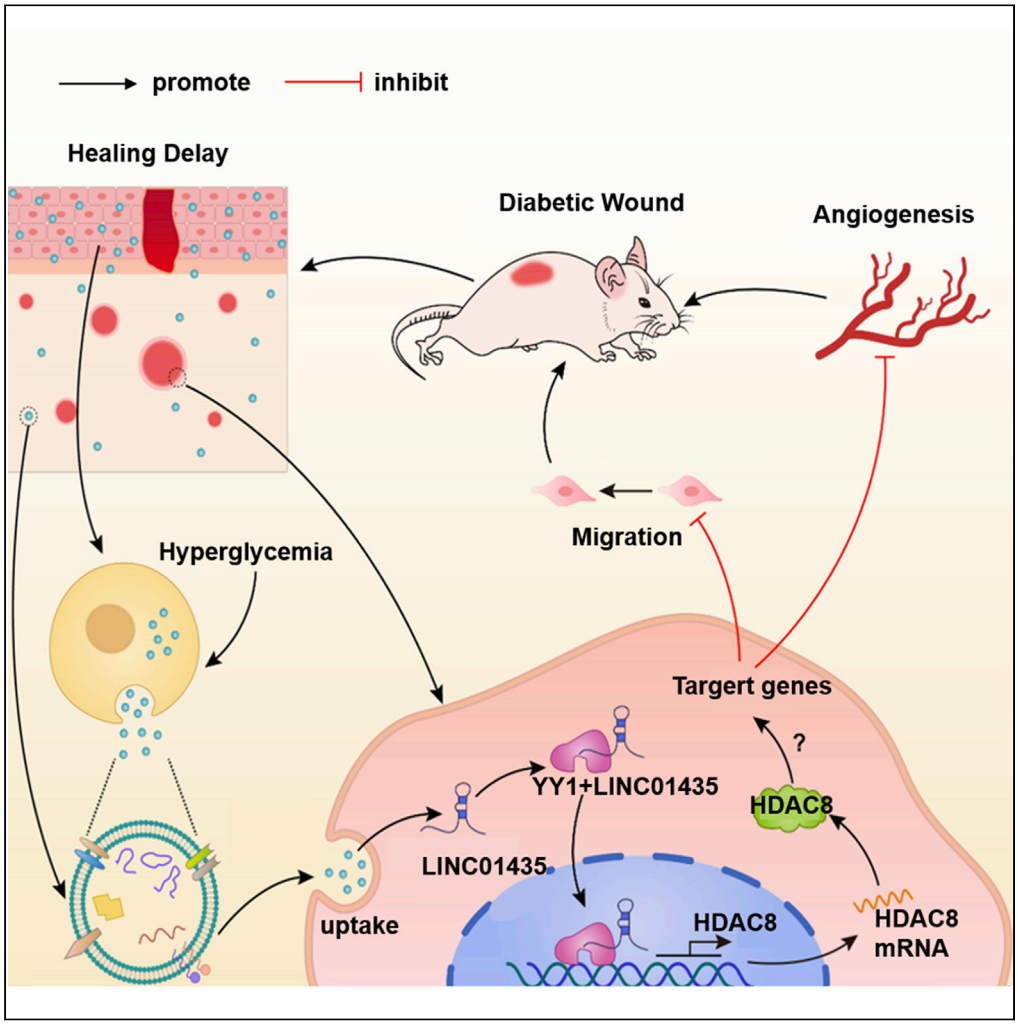

Wan Fu, Diefei Liang, Xiaoying Wu, ..., Sifan Chen, Li Yan, Meng Ren

renmeng80@139.com

Highlights

HG-Exos derived from HaCaT cells can suppress wound healing in diabetic skin

Exosomal LINC01435 plays an important role in diabetic wound healing

LINC01435 inhibits angiogenesis through the YY1/HDAC8 pathway

Fu et al., iScience *25*, 104006
April 15, 2022 © 2022
https://doi.org/10.1016/j.isci.2022.104006

iScience

CellPress
OPEN ACCESS

Article

Long noncoding RNA LINC01435 impedes diabetic wound healing by facilitating YY1-mediated HDAC8 expression

Wan Fu,[1,2] Diefei Liang,[1,2] Xiaoying Wu,[1,2] Hongxing Chen,[1,2] Xiaosi Hong,[1,2] Jiahuan Wang,[1,2] Tianxin Zhu,[1,2] Tingting Zeng,[1,2] Weijie Lin,[2,3] Sifan Chen,[2,3] Li Yan,[1,2] and Meng Ren[1,2,4,*]

SUMMARY

Abnormal interactions between skin cells play an important role in the dysregulation of diabetic wound recovery. Exosomes are cell-derived lipid nanoparticles that transport messages between cells, and isolating and identifying potential therapeutic noncoding RNAs from exosomes is very important. We demonstrated that treatment with Exos from high glucose-pretreated immortalized human epidermal (HaCaT) cells (HG-Exos) could delay the wound healing process in diabetic mice. Further analysis indicated the Exo-mediated uptake of LINC01435 in recipient human umbilical vein endothelial cells (HUVECs) changes the subcellular localization of the transcription factor Yin Yang 1 (YY1) and cooperates with YY1 to upregulate the expression of histone deacetylases (HDACs)8, resulting in decreased tube formation and ability of HUVECs to migrate, thus angiogenesis was inhibited. These results suggest that LINC01435/YY1/HDAC8 may be an important signaling pathway affecting the recovery of diabetic wounds, which makes it a potential target for the treatment of diabetic foot ulcers.

INTRODUCTION

Type 2 diabetes mellitus (T2DM) is a heterogeneous chronic disease caused by multilayer interactions between genetic predisposition and environmental/lifestyle factors (DeFronzo et al., 2015). Up to 4% of diabetic patients may be affected by diabetic foot ulcers. Although many treatment strategies for chronic wounds have been attempted, the cure rate remains low, with approximately 28% of patients requiring lower limb amputation (Bakker et al., 2016; Falanga, 2005). Wound healing is a complex process involving well-orchestrated biological and molecular events, such as cell migration and proliferation, extracellular matrix (ECM) deposition and remodeling, and angiogenesis. Abnormal interactions between skin cells play an important role in the dysregulation of diabetic wound recovery (Galkowska et al., 2006). There is ample evidence on the role of keratinocyte–fibroblast interactions in the wound-healing process. However, the relationship between keratinocytes and vascular endothelial cells remains unknown.

Exosomes are extracellular vesicles produced by the inward budding of many types of cells through late endosomes and have been recognized as an important cell-to-cell communication tool that delivers miRNAs, mRNAs, or proteins from sender cells to recipient cells, influencing intracellular signaling and various biological processes (Skotland et al., 2020; Zhao et al., 2020). It has been shown that exosomes derived from human endothelial progenitor cells, human umbilical cord blood, and mesenchymal stem cells significantly promote wound healing by regulating the function of human fibroblasts (HFBs) and human umbilical vein endothelial cells (HUVECs) (Hu et al., 2018; Shabbir et al., 2015; Zhang et al., 2016). LncRNAs are present in exosomes, suggesting that lncRNAs may also be loaded into exosomes during intercellular communication to further regulate gene expression in recipient cells (Cech and Steitz, 2014). Research has shown that exosomes carry long noncoding RNAs (lncRNAs) that are transmitted between different cells and regulate the function of receptor cells (Guttman et al., 2013; Huarte et al., 2010). However, whether keratinocytes mediate the recovery of diabetic wounds by regulating the function of vascular endothelial cells through secreting exosomal lncRNAs remains unclear.

Previous studies have reported that Notch signaling plays an important role in the process of angiogenesis (Lim et al., 2019). High glucose disrupts Notch angiogenesis signaling in endothelial cells and eventually

[1]Department of Endocrinology, Sun Yat-Sen Memorial Hospital, Sun Yat-Sen University, 107 Yanjiang West Road, Guangzhou 510120, China

[2]Guangdong Provincial Key Laboratory of Malignant Tumor Epigenetics and Gene Regulation, Sun Yat-Sen Memorial Hospital, Sun Yat-Sen University, 107 Yanjiang West Road, Guangzhou 510120, China

[3]Medical Research Center, Sun Yat-Sen Memorial Hospital, Sun Yat-Sen University, Guangzhou 510120, China

[4]Lead contact

*Correspondence: renmeng80@139.com

https://doi.org/10.1016/j.isci.2022.104006

leads to diabetic wounds that are difficult to heal (Ho et al., 2018). Histone deacetylases (HDACs), an important component of the NOTCH signaling pathway, are functional groups that catalyze the acetylation of histone and nonhistone lysine residues (Mobley et al., 2017). HDAC8 is a class I HDAC that acetylates histones H3 and H4 on nonspecific lysine residues and plays a role in a variety of disease processes (Zhou et al., 2020). HDAC8 binds and deacetylates the K62 residue of PKM2, which further promotes the insertion of PKM2 into the nucleus and the binding of β-catenin, thereby promoting CCND1 gene transcription and HCC cell cycle progression (Rinn and Chang, 2012). HDAC8 can inhibit the proliferation and migration of cancer cells by synergistic action with Smad3/4, which has a certain potential to treat triple-negative breast cancer (Shi et al., 1991). However, the role of HDAC8 in angiogenesis in diabetic foot wound healing has rarely been reported.

Here, we studied the functional roles of HG-Exos both *in vitro* and *in vivo* and explored the mechanism through which LINC01435 derived from HG-Exos regulates HDAC8 expression and influences vascular endothelial cell phenotypes in diabetic wound healing.

RESULTS

Characterization of the HaCaT-derived exosomes

Nanosight analysis demonstrated that the average sizes of NG-Exos and HG-Exos both ranged from approximately 50 to 200 nm (Figures 1A and 1B). Cup-shaped or sphere-shaped and membrane-bound vesicles were observed via TEM, as shown in Figure 1C. The results of western blotting confirmed the presence of exosomal surface markers, including CD9 and TSG101, in NG-Exos and HG-Exos, with Grp94 as a negative control (Figure 1D). In addition, NTA demonstrated that the particle concentration of HG-Exos was similar to that of NG-Exos (Figure 1E). To further investigate whether HaCaT-Exos could be internalized by HUVECs, exosomes were labeled with the red fluorescent lipid dye PKH26 and then incubated with HUVECs. The laser scanning confocal microscopy results showed that PKH26 was present in HaCaT-Exo-treated HUVECs (Figure 1F), suggesting that exosome endocytosis by HUVECs had occurred.

HG-Exos inhibit the migration and tube formation of HUVECs *in vitro* and suppress cutaneous wound healing in db/db mice *in vivo*

Next, we wanted to explore the hypothesis that HG-Exos derived from HaCaT cells impair local angiogenesis and can suppress wound healing in diabetic skin. As shown in Figures 2A and 2B, the cell migration and tube formation abilities of HUVECs decreased significantly in the group of exosome stimulation (A) or exosome stimulation under high glucose conditions (B). There were significant inhibitory effects of coculture under high glucose conditions on endothelial cell migration and tube formation were assessed using migration and tube formation (Figure S1D). However, there were no differences in the proliferation and apoptosis capacity of HUVECs incubated with HaCaT cells and HaCaT-Exos (Figures S1A–S1C, S1E, and S1I). Type 2 diabetic mice (db/db mice) and control mice (wild-type, WT mice) weighing 20–40 g were randomly divided into three groups and treated with vehicle control (PBS), NG-Exos, or HG-Exos. As shown in Figure 2C, treatment with HG-Exos significantly reduced the wound closure ratio of mice at Days 3, 6, and 9. We next examined the protein expression of an angiogenesis marker (CD31) in the wounds of the six groups. The HG-Exos group exhibited lower CD31 expression at the wound site than that of the control and NG-Exos groups in both WT and db/db mice by immunohistochemistry (Figure 2D), indicating that treatment with HG-Exos suppressed microvascularization and angiogenesis in cutaneous wounds. Immunofluorescence assay showed that the expression level of CD31 and vimentin in dermal vascular endothelial cells was downregulated in db/db mice under HG-Exos stimulation (Figure S1J). Under the same conditions, the expression of Ecadherin in skin microvessels was upregulated. Taken together, these findings suggested that treatment with HG-Exos derived from HaCaT cells could negatively affect the biological functions of HUVECs *in vitro* and contribute to a significant delay in the wound healing of db/db mice.

HG-Exos inhibit HUVECs tube formation *in vitro* through Exo-LINC01435

First, microarray technology was used to analyze the differences between the lncRNA expression profiles of HaCaT-derived Exos with and without AGE treatment (Figure S2A). Five lncRNAs (CPB2-AS1, DARS-AS1, G001249, LINC01435, and MIR22HG) with significant differences (fold changes ≥ 2 and p value < 0.05) were selected. Then, real-time PCR analysis was used to confirm that these lncRNAs were indeed differentially expressed in HaCaT cells treated with high glucose and HG-Exos versus HaCaT cells treated with high

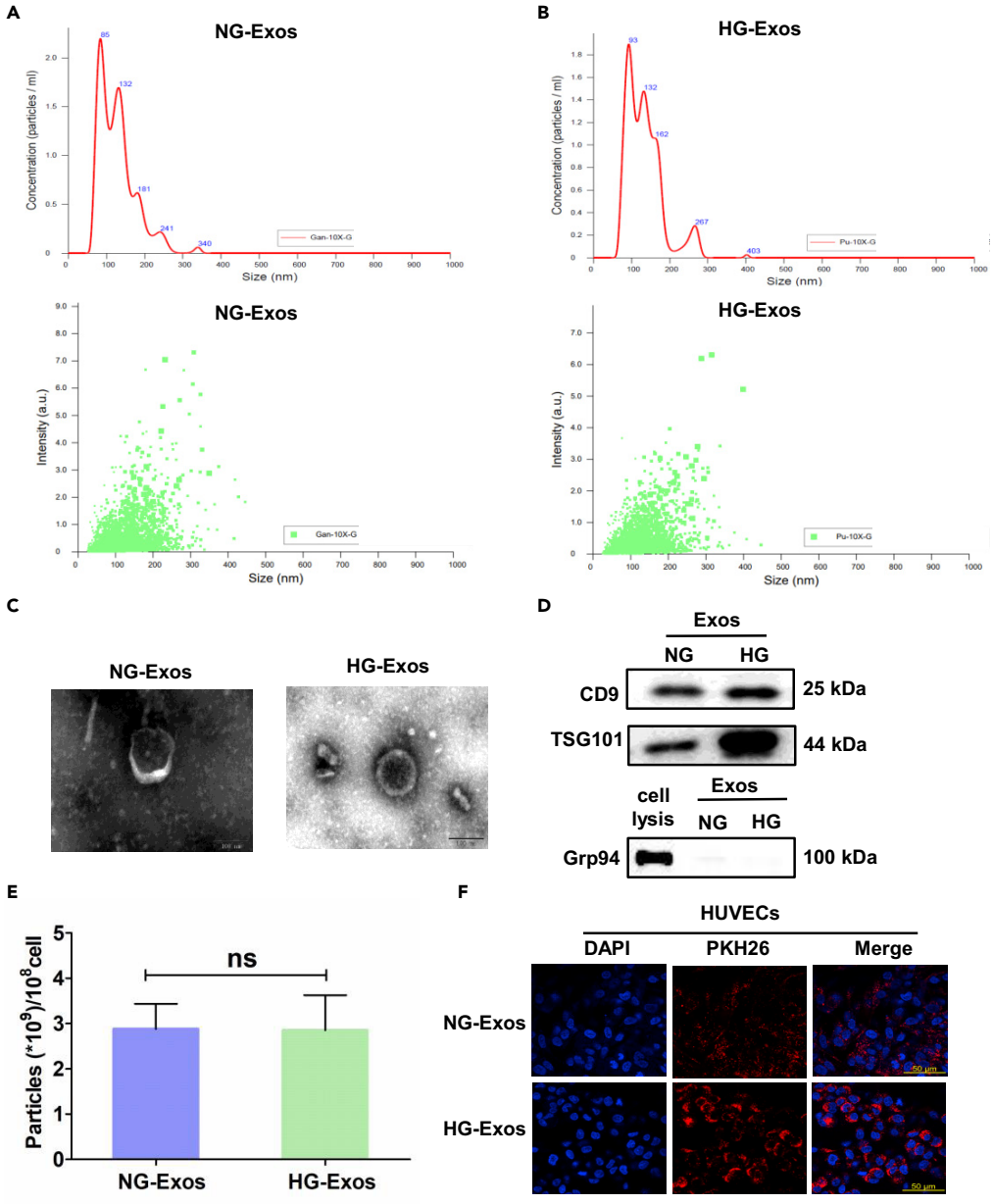

Figure 1. Characterization of the HaCaT-derived exosomes

(A and B) NanoSight analysis demonstrated that the average sizes of NG-Exos (A) and HG-Exos (B) both ranged from approximately 50 to 200 nm.

(C) The ultrastructure of the two kinds of exosomes was observed by transmission electron microscopy (TEM), which showed cup-shaped or spherical membranous vesicles. Scale bars, 100 nm in (C).

(D) Western blotting was used to analyze the protein levels of exosomal markers (CD9 and TSG101) and the negative control marker (Grp94).

(E) NG-Exo and HG-Exo particle concentrations were determined using the NTA method. Data are expressed as mean ± standard deviation, n = 3. Two-tailed unpaired-samples *t*-test; ns $p > 0.05$.

(F) Exosomes labeled with the red fluorescent lipid dye PKH26 were coincubated with HUVECs and photographed under a laser scanning confocal microscope. Exosomes and cell nuclei were stained red and blue, respectively. Scale bars, 50 μm in (F).

mannitol and NG-Exos (Figure 3A). The expression of candidate lncRNAs in HUVECs was quantified after coculture with or without HaCaT cells (Figure S2B) and treatment with HG-Exos or NG-Exos (Figure 3B) through real-time PCR. We identified a lncRNA, LINC01435, which was highly expressed in all the

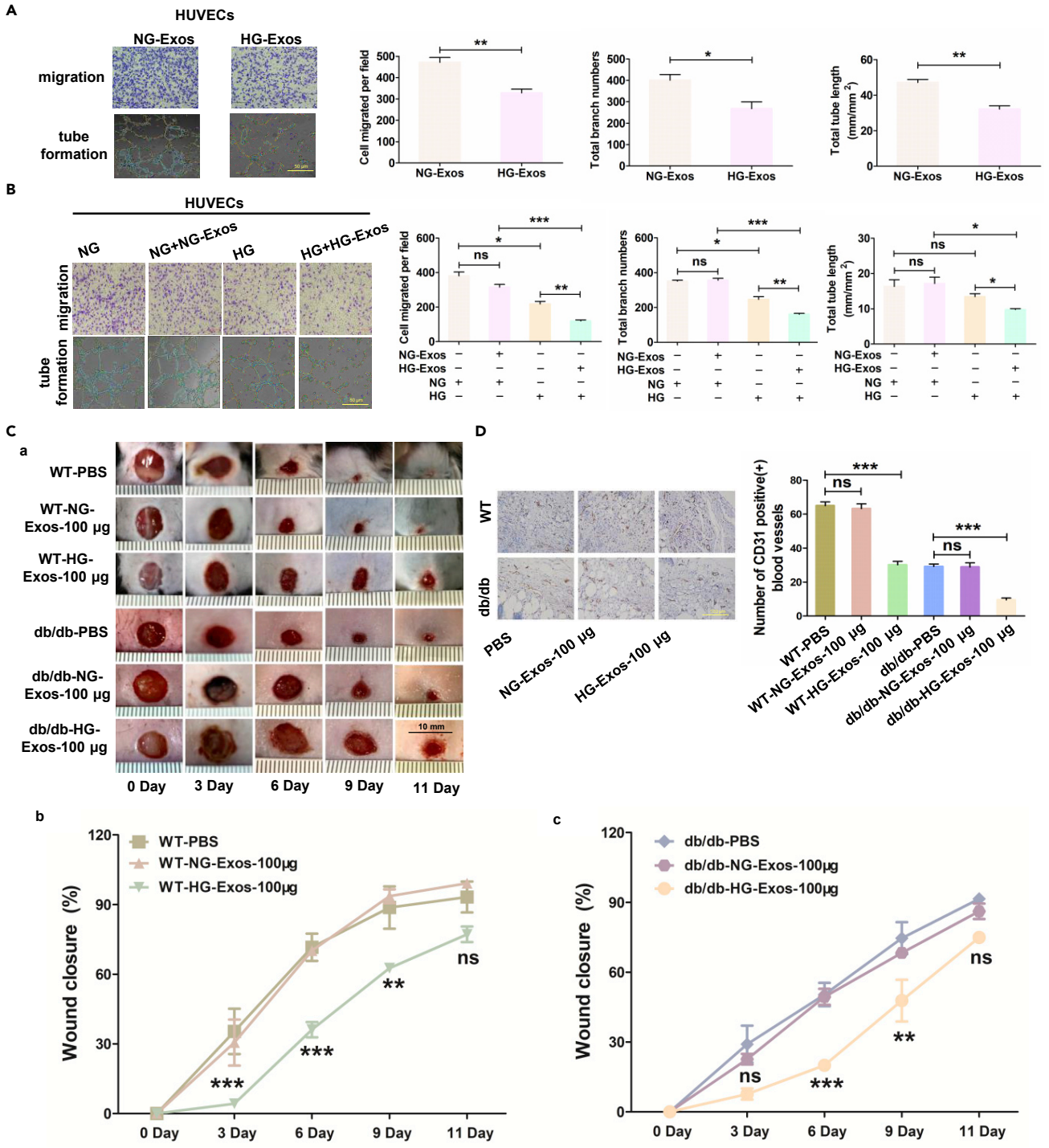

Figure 2. HG-Exos inhibit the migration and tube formation of HUVECs *in vitro* and suppress cutaneous wound healing in db/db mice *in vivo*

(A and B) The effects of exosome stimulation (A) or exosome stimulation under high glucose conditions (B) on endothelial cell migration and tube formation were assessed using migration and tube formation experiments. Data are expressed as mean ± standard deviation, n = 3. Student's *t* test; ns $p > 0.05$, *$p < 0.05$, **$p < 0.01$, and ***$p < 0.001$. The scale bars represent 100 μm for migration and 50 μm for tube formation.

(C) (a) General view of the cutaneous wounds from different treatment groups at 0 days, 3 days, 6 days, 9 days, and 11 days after wounding. The wound closure rates of the six groups were quantified using digital images evaluated by ImageJ software (National Institutes of Health). Quantification of wound closure in n = 6 (WT-PBS), n = 7 (WT-NG-Exos-100 μg), n = 7 (WT-HG-Exos-100 μg), n = 6 (db/db-PBS), n = 6 (db/db- NG-Exos-100 μg), and n = 8 (db/db- HG-Exos-100 μg) wounds per group was performed with GraphPad Prism software. Scale bars, 10 mm in (a). The significant difference between groups WT-PBS

Figure 2. *Continued*

and WT-HG-Exos-100 μg is denoted in (b) and that between group db/db-PBS and group db/db- HG-Exos-100 μg is denoted in (c). The data were presented as mean ± SEM in (b and c) and analyzed by one-way ANOVA with Dunnett's T3 multiple comparison test in (b and c). ***$p < 0.001$; **$p < 0.01$; *$p < 0.05$; ns $p > 0.05$.

(D) CD31 immunohistochemistry staining of wound sites with different treatments was performed using microscopic imaging sections (Nikon). CD31 staining was performed by quantifying the number of $CD31^+$ cells to assess wound microvascularization in 6 randomized fields, counting vessels with diameters of 2–110 μm as individual vessels. Data are the means ± standard deviation of three independent experiments. Two-tailed unpaired-samples *t*-test with Welch's correction; ns $p > 0.05$, ***$p < 0.001$. Scale bars, 100 μm in (D).

treatments described above. In addition, the LINC01435 expression level of HaCaT cells was higher than that of HUVECs under normal glucose and high glucose conditions (Figure S2C). To investigate the role of LINC01435, we used nucleoplasmic isolation of cellular RNA and FISH to confirm its upregulation in HUVECs cocultured with HaCaT cells or HG-Exos (Figure S2D). Transwell assays and tube formation tests showed that when HUVECs were treated with HaCaT cells or HG-Exos together with SM-LINC01435, a mixture of three siRNA and three ASO is used to knock down the expression of LINC01435 in cytoplasm and nucleus, the negative effect of HaCaT cells (Figure S2E) or HG-Exos (Figure 3C) on the cell migration and tube formation of HUVECs was reversed. However, SM-LINC01435 together with treatment with HaCaT cells or HG-Exos did not affect the proliferation and apoptosis capacity of HUVECs (Figures S2F–S2H). To further elucidate the role of LINC01435 in the inhibition of angiogenesis by HG-Exos, HUVECs were treated with the pcDNA3.1-LINC01435, vector as a control, whereby the former significantly increased the expression of LINC01435 (Figure S2I). The results of transwell and tube formation assays confirmed the ability of LINC01435 to suppress the migration and tube formation of HUVECs (Figures 3D and 3E). However, there were no significant differences in the proliferation and apoptosis capacity of HUVECs between the pcDNA3.1-LINC01435 and control groups (Figures S2J–S2L). Taken together, these results confirmed the ability of HG-Exos to inhibit HUVEC function through Exo-LINC01435 *in vitro*.

HDAC8 contributes to the inhibition of angiogenesis by Exo-LINC01435

In this study, we screened genes to identify whether HDAC8/NOTCH signaling was responsible for the negative effect of Exo-LINC01435 on angiogenesis. The qPCR and western blotting results showed that the mRNA and protein levels of HDAC8 were upregulated by coculture with HaCaT cells (Figures S3A and S3B) or HG-Exos and overexpression of LINC01435 (Figures 4A–4C). The immunofluorescence analysis showed that the protein levels of HDAC8 were upregulated (Figures S3C and S3D). We downregulated its expression via transfection with siRNAs targeting HDAC8, and the effect could be reversed by LINC01435 overexpression (Figure 4D). Transwell and tube formation assays indicated that siRNA-HDAC8 promoted cell migration and tube formation, whereas the overexpression of LINC01435 partially reversed the proangiogenic effects of siRNA-HDAC8-2# on HUVECs (Figure 4E). In addition, there were no significant differences in the proliferation and apoptosis ability of HUVECs between the siRNA-HDAC8-2# group, LINC01435 overexpression group, and control group (Figures S3E–S3G). Immunofluorescence assay showed that the expression level of HDAC8 in dermal vascular endothelial cells was upregulated in diabetic foot skin tissue samples and db/db mice (Figure 4F). Taken together, our results showed that HDAC8 contributes to the inhibition of angiogenesis by Exo-LINC01435.

LINC01435 upregulates the expression of HDAC8 at the transcription level by recruiting YY1 transcription factors into the nucleus

After searching for LINC01435-interacting proteins via protein mass spectrometry and silver staining, the critical transcription factor YY1 was recognized as a LINC01435-binding protein (Figures S4A and S4B). The western blot shown in Figure 5A confirmed the interaction between LINC01435 and YY1. RIP assays performed with an anti-YY1 antibody also verified the interaction between YY1 and LINC01435 (Figure 5B). No significant difference was found in the mRNA and protein levels of YY1 after LINC01435 overexpression (Figure 5C). Immunofluorescence staining revealed a higher abundance of YY1 in the nucleus after LINC01435 was overexpressed, indicating that YY1 was recruited into the nucleus by LINC01435 (Figure 5D). Furthermore, we found that LINC01435 overexpression led to a clear upregulation of HDAC8 mRNA and protein expression, and the inhibition of YY1 via siRNA partially reversed the effects of LINC01435 overexpression on HDAC8 in HUVECs (Figure 5E). The promoter region sequence of HDAC8 and the possible binding site of YY1 were predicted by the websites UCSC, JASPAR, and PROMO (Figures 5F and 5G). A luciferase reporter assay was performed to verify whether YY1 could bind directly to putative target sites in the HDAC8 promoter (Figure 5H). The results indicated that LINC01435 overexpression significantly enhanced the luciferase activity of the pGl3–566-wt construct and the inhibition of YY1 via

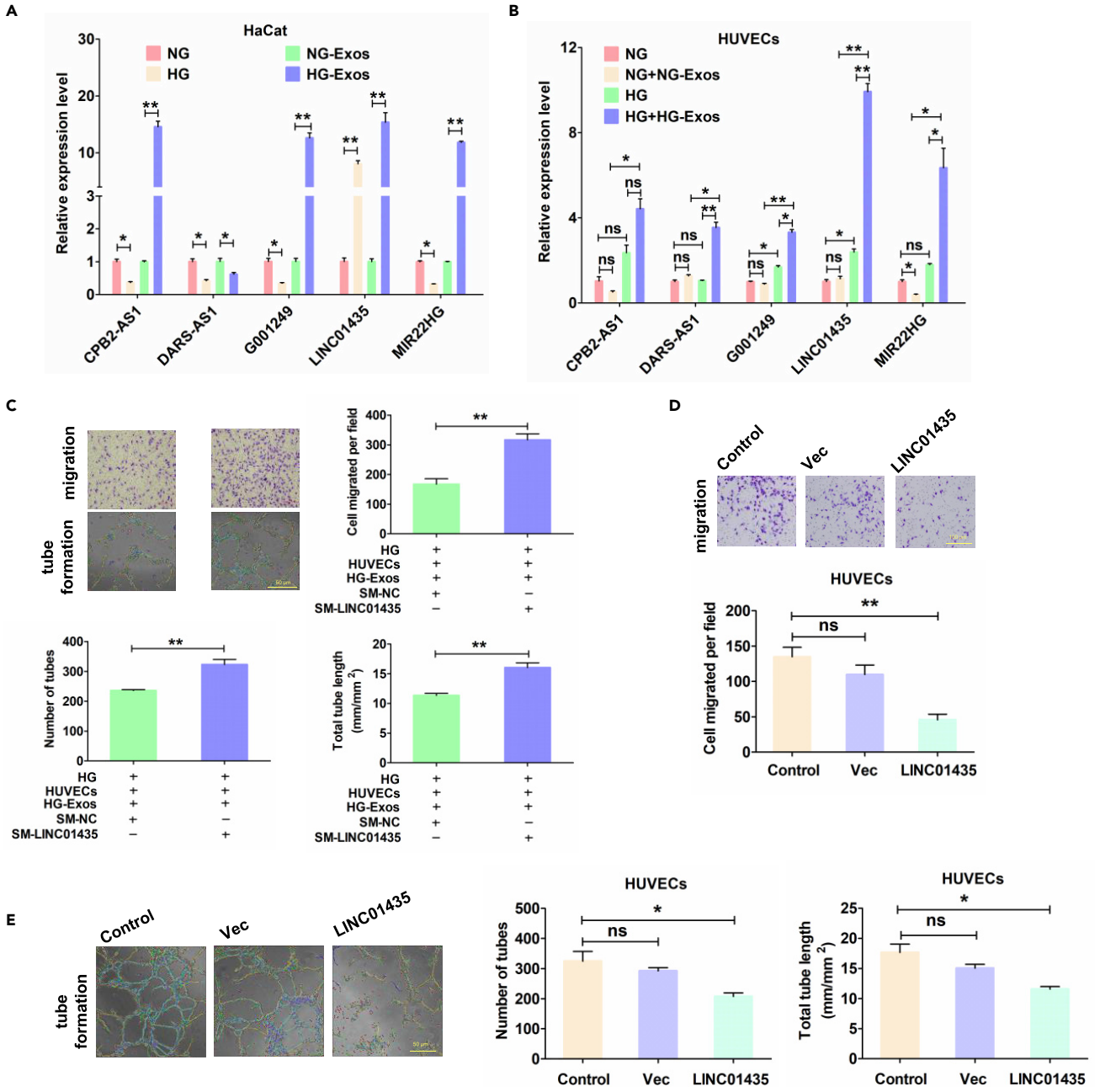

Figure 3. HG-Exos inhibit HUVECs tube formation *in vitro* through exo-LINC01435

(A) The levels of differentially expressed lncRNAs in HaCaT cells and exosomes were determined by qPCR after 48 h of treatment with normal glucose and high glucose. Data are expressed as mean ± standard deviation, n = 3. Student's *t* test; ns $p > 0.05$, *$p < 0.05$, **$p < 0.01$.

(B) LncRNAs differentially expressed in HUVECs were detected by qPCR after exosome stimulation. Data are expressed as mean ± standard deviation, n = 3. Student's *t* test; ns $p > 0.05$, *$p < 0.05$, **$p < 0.01$.

(C) After exosome stimulation of HUVECs, smart silencing was used to knock down LINC01435 to detect the migration of HUVECs and the change in migration and tube formation ability. Data are expressed as mean ± standard deviation, n = 3. Student's *t* test; *$p < 0.05$, **$p < 0.01$. The scale bars represent 50 μm for migration and 50 μm for tube formation.

(D) The Transwell assay was used to detect the changes in endothelial cell migration following overexpression of LINC01435. Data are expressed as mean ± standard deviation, n = 3. Student's *t* test; ns $p > 0.05$, **$p < 0.01$. Scale bars, 100 μm in (D).

(E) The effect of LINC01435 overexpression on endothelial tubule formation was assessed using the ventricular tubule assay. Data are expressed as mean ± standard deviation, n = 3. Student's *t* test; ns $p > 0.05$, *$p < 0.01$. Scale bars, 50 μm in (E).

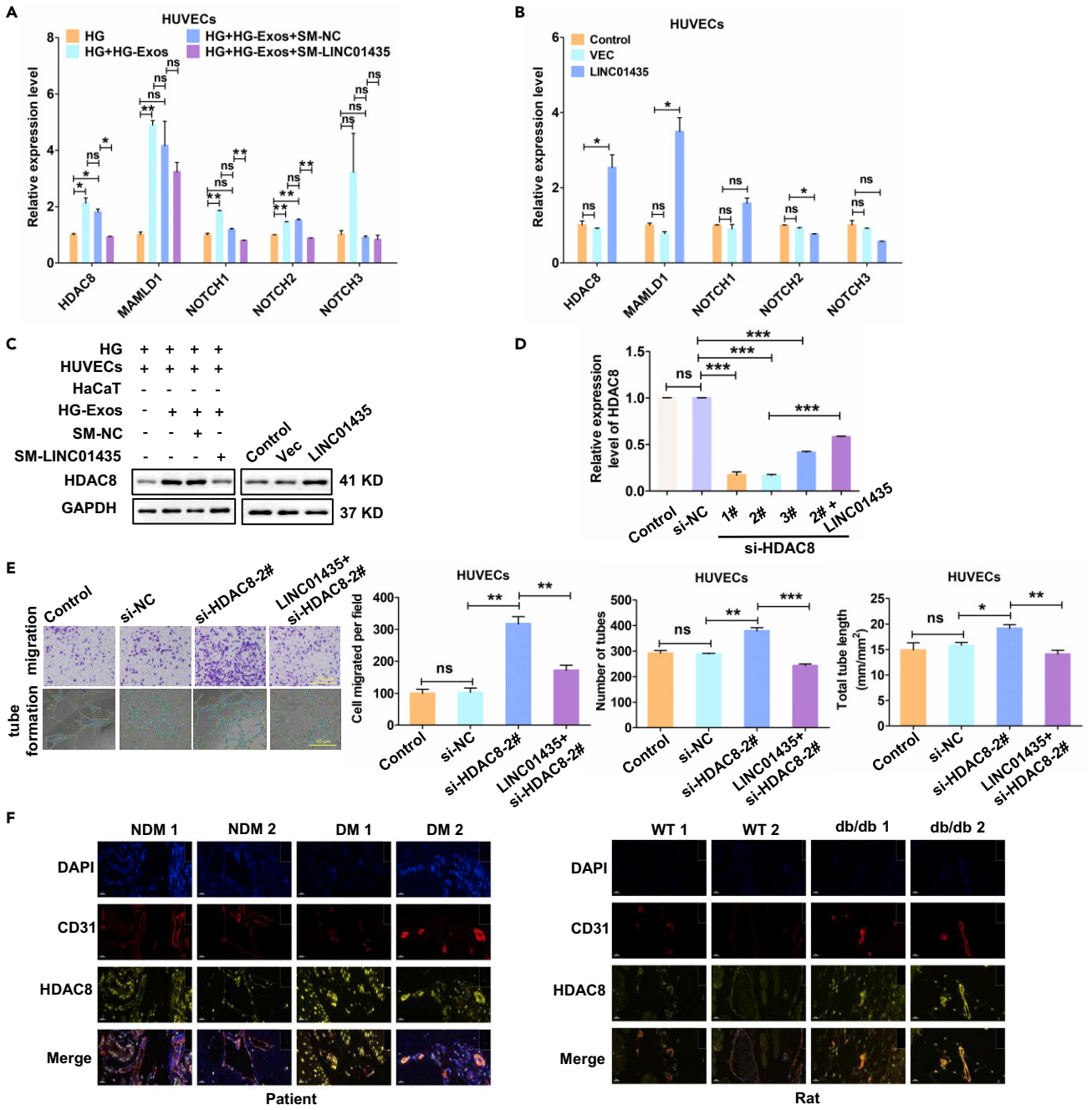

Figure 4. HDAC8 contributes to the inhibition of angiogenesis by exo-LINC01435

(A) After exosome stimulation, LINC01435 was knocked down, and qPCR was used to verify the mRNA expression levels of genes related to the Notch signaling pathway in endothelial cells. Data are expressed as mean ± standard deviation, n = 3. Student's *t* test; ns $p > 0.05$, *$p < 0.05$, **$p < 0.01$.

(B) After LINC01435 was overexpressed, qPCR was used to verify the mRNA expression levels of target genes related to the Notch signaling pathway in endothelial cells. Data are expressed as mean ± standard deviation, n = 3. Student's *t* test; ns $p > 0.05$, *$p < 0.05$.

(C) Western blot analysis was used to determine the changes in the protein expression level of HDAC8 after exosomal stimulation and overexpression of LINC01435. Western blotting was performed with HDAC8 and GAPDH antibodies.

(D) HDAC8 was knocked down, and LINC01435 was overexpressed at the same time. The changes in HDAC8 mRNA expression were detected by qPCR. Data are expressed as mean ± standard deviation, n = 3. Student's *t* test; ns $p > 0.05$, ***$p < 0.001$.

(E) The effects of HDAC8 knockdown and simultaneous overexpression of LINC0435 on endothelial cell migration and angiogenesis ability were examined using transwell and tube-formation assays. Data are expressed as mean ± standard deviation, n = 3. Student's *t* test; ns $p > 0.05$, *$p < 0.05$, **$p < 0.01$, ***$p < 0.001$. The scale bars represent 100 μm for migration and 50 μm for tube formation.

(F) IF detection of CD31/HDAC8 expression in diabetic foot skin tissue samples and db/db mice. Scale bars, 20 μm in (F).

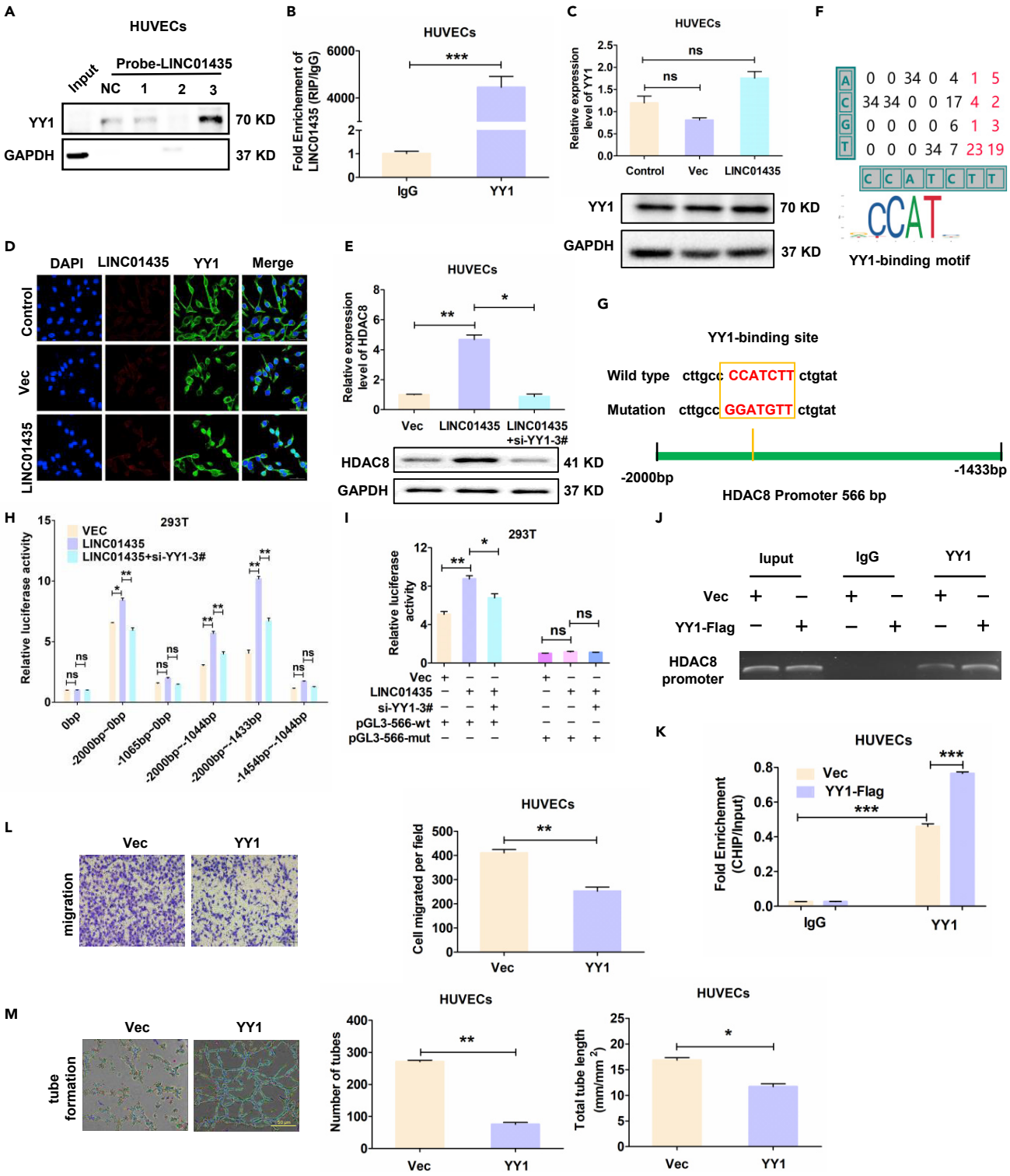

Figure 5. LINC01435 upregulates the expression of HDAC8 at the transcription level by recruiting YY1 transcription factors into the nucleus

(A) A protein pull-down assay in HUVECs with LINC01435 as the probe revealed that the transcription factor YY1 can bind to LINC01435. Western blotting was performed with YY1 and GAPDH antibodies.

(B) The RIP test was performed with an antibody against YY1 (IgG as a control), and qPCR verified that LINC01435 could bind to YY1. Data are expressed as mean ± standard deviation, n = 3. Student's *t* test; ***p < 0.001.

Figure 5. *Continued*

(C) After overexpression of LINC01435, the mRNA and protein levels of YY1 were quantified by qPCR and western blotting. Data are expressed as mean ± standard deviation, n = 3. Student's *t* test; ns $p > 0.05$.

(D) After overexpressing LINC01435, the localization of YY1 in the cytoplasm or nucleus was detected by immunofluorescence staining. Scale bars, 50 μm in (D).

(E) After LINC01435 was overexpressed, YY1 was knocked down, and the changes in HDAC8 mRNA and protein levels were detected by qPCR and western blot analysis. Data are expressed as mean ± standard deviation, n = 3. Student's *t* test; ns $p > 0.05$, *$p < 0.05$, **$p < 0.01$.

(F and G) The promoter region sequence of HDAC8 and the possible binding site of YY1 were predicted by the websites JASPAR (F), UCSC (G), and PROMO (G).

(H) The regulation of different fragment lengths in the HDAC8 promoter region after the overexpression of LINC01435 and simultaneous knockdown of YY1 were detected using the dual luciferase reporter assay. Data are expressed as mean ± standard deviation, n = 3. Student's *t* test; ns $p > 0.05$, *$p < 0.05$, **$p < 0.01$.

(I) The regulation of the promoter region of HDAC8 by LINC01435/YY1 was further verified by mutating segment 566 and conducting the same dual luciferase reporter assay with the mutated variant. Data are expressed as mean ± standard deviation, n = 3. Student's *t* test; ns $p > 0.05$, *$p < 0.05$, **$p < 0.01$.

(J and K) Chromatin immunoprecipitation (ChIP) confirmed that YY1 could directly bind to the promoter region of HDAC8. Data are expressed as mean ± standard deviation, n = 3. Student's *t* test; **$p < 0.01$, ***$p < 0.001$.

(L) The transwell assay was used to detect the changes in endothelial cell migration following overexpression of YY1. Data are expressed as mean ± standard deviation, n = 3. Student's *t* test; ns $p > 0.05$, **$p < 0.01$. Scale bars, 100 μm in (L).

(M) The effect of YY1 overexpression on endothelial tubule formation was assessed using the ventricular tubule assay. Data are expressed as mean ± standard deviation, n = 3. Student's *t* test; ns $p > 0.05$, *$p < 0.01$. Scale bars, 50 μm in (M).

siRNA partially reversed this effect in 293T cells. In contrast, no such effect was found in the mutated construct, indicating that there were interactions among LINC01435, YY1, and HDAC8 at this putative binding site (Figure 5I). Chromatin immunoprecipitation (ChIP) and ChIP-qPCR were further performed to detect the binding of YY1 to the HDAC8 promoter region (Figures 5J and 5K). The results of transwell and tube formation assays confirmed the ability of YY1 to suppress the migration and tube formation of HUVECs (Figures 5L and 5M). However, there were no significant differences in the proliferation and apoptosis capacity of HUVECs between YY1 and control groups (Figures S4C–S4E). Immunofluorescence assay showed that the expression level of YY1 in dermal vascular endothelial cells had no change in diabetic foot skin tissue samples and db/db mice (Figure S4F). Taken together, the results demonstrated that LINC01435 upregulated the expression of HDAC8 at the transcriptional level by recruiting the transcription factor YY1 into the nucleus.

LINC01435 inhibits angiogenesis through the YY1/HDAC8 pathway

To further elucidate the role of the YY1/HDAC8 signaling pathway in the suppression of angiogenesis by LINC01435, the migration and tube formation abilities of HUVECs were enhanced by siRNA-YY1-3#, indicating that the inhibition of YY1 was able to partially reverse the antiangiogenic effects of LINC01435 in HUVECs Figure 6A). Notably, the enhanced cell migration and tube formation of YY1-knockdown cells were partially blocked by HDAC8 overexpression (Figure 6A), but HDAC8 overexpression had no significant influence on the proliferation and apoptosis of HUVECs (Figures S5A–S5C). Microarray technology and FISH/IF were used to analyze LINC01435/YY1/HDAC8 expression in human tissue samples (Figures 6B and 6C). In addition, the results of the response experiment after co-transfecting of si-HDAC8-2#, YY1, and SM-LINC01435 are shown in Figure S6, and the results are consistent with the trend in Figure 6. Crucially, this study indicates that LINC01435 was delivered into HUVECs by HG-Exos derived from HaCaT cells, and the upregulation of LINC01435 impaired the migration and tube formation of HUVECs through the YY1/HDAC8 pathway (Figure 7).

DISCUSSION

In this study, our results suggest that keratinocyte-derived exosomal LINC01435 may regulate the function of vascular endothelial cells, which in turn influence the recovery of diabetic wounds. We screened genes to identify that HDAC8 was responsible for the negative effect of Exo-LINC01435 on angiogenesis. Through searching for LINC01435-interacting proteins via protein mass spectrometry and western blotting, we found that LINC01435 could bind with YY1. Further luciferase reporter assays and CHIP-qPCR studies showed that LINC01435 upregulated the expression of HDAC8 at the transcriptional level by recruiting the transcription factor YY1 into the nucleus.

In the physiological process of skin wound healing, various cells in the skin microenvironment perform their respective roles, interacting with each other and the extracellular matrix to jointly complete the process of

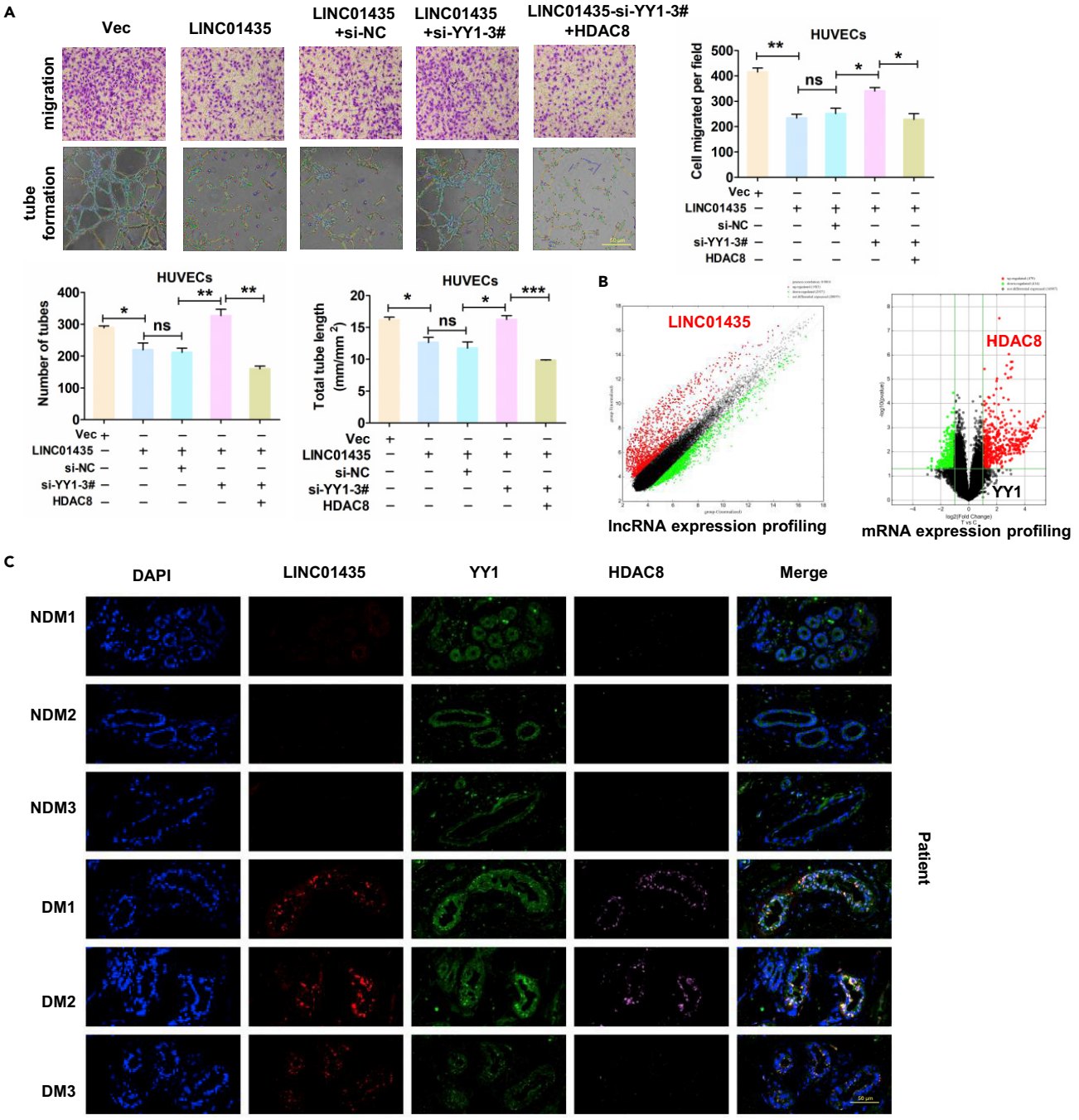

Figure 6. LINC01435 inhibits angiogenesis through the YY1/HDAC8 pathway

(A) The effects of LINC0435, si-YY1, and HDAC8 cotransfection on endothelial cell migration and angiogenesis ability were detected by Transwell and tube formation assays. Data are expressed as mean ± standard deviation, n = 3. Student's *t* test; ns $p > 0.05$, *$p < 0.05$, **$p < 0.01$, ***$p < 0.001$. The scale bars represent 100 μm for migration and 50 μm for tube formation.

(B) Microarray technology was used to analyze LINC01435/YY1/HDAC8 expression in the great saphenous vein in ordinary people or diabetic patients.

(C) FISH/IF detection of LINC01435/YY1/HDAC8 expression in diabetic foot skin tissue samples. Scale bars, 50 μm in (C).

tissue repair. Studies have shown that keratinocytes are the key cells in the skin immune microenvironment (Falanga, 2005; Lee et al., 2011; Yu et al., 2020). The formation of new blood vessels is essential for the regeneration of skin tissue during wound healing, which plays an important role by delivering nutrients, oxygen, and growth factors to the injury site (Tsai et al., 2018). Abnormal changes such as impaired

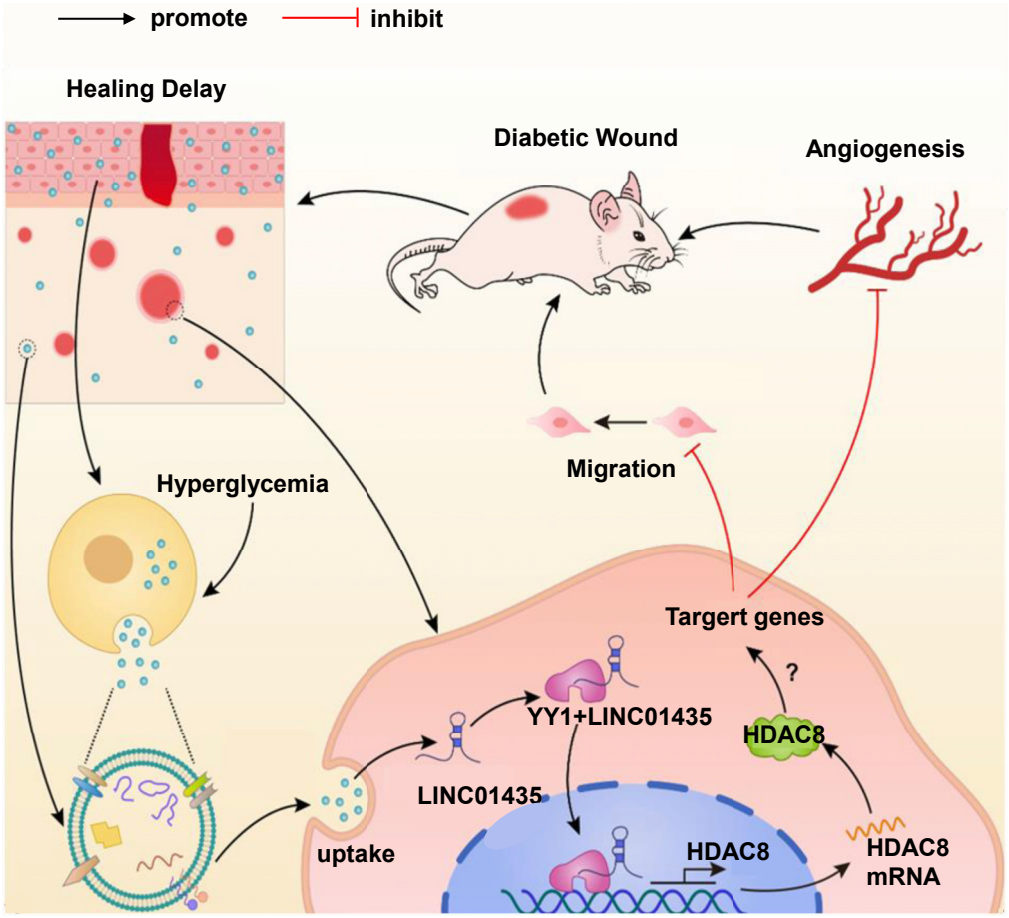

Figure 7. Schematic diagram of the proposed model of LINC01435/YY1/HDAC8 in the diabetic wound healing process schematic diagram of the role of keratinocyte-derived LINC01435 in the dysfunction of human skin endothelial cells under hyperglycemic conditions typical of diabetes

angiogenic responses, reduced granulation tissue volume, and overactivation of the matrix metalloproteinase system (MMPs) that disrupts the balance of extracellular matrix deposition and remodeling all ultimately lead to difficulties in wound healing (Pefanis et al., 2015; Xu et al., 2020).

Studies have shown that exosomes are involved in the development of diabetes and its related complications and may provide us with new biomarkers for the early diagnosis and stratification of patients at risk for diabetes, thus allowing timely implementation of more personalized treatment (Bao et al., 2018; Deardorff et al., 2012; Limbourg et al., 2005; Lindner et al., 2001). In recent years, exosomes, exosome miRNAs, and lncRNAs associated with diabetes have shown promise in the pathology and diagnosis of diabetes, which may help us to better understand the exact role of exosomes in the development of diabetes (An et al., 2020). It has been shown that miRNA-24–3p is enriched in circulating exosomes (DIA-Exos) in diabetic patients and enhances the *in vitro* function of HUVECs by upregulating PIK3R3 expression (Emmons et al., 2019). Mesenchymal stem cell-derived exosomal lncRNA H19 promotes wound healing of diabetic foot ulcers by upregulating PTEN by sponging microRNA-152–3p (Li et al., 2020). We identified that LINC01435 was highly expressed in HUVECs cocultured with HaCaT cells or HG-Exos. Furthermore, our results suggest that keratinocyte-derived exosomal LINC01435 inhibits HUVEC tube formation and migration under high glucose conditions, thereby inhibiting angiogenesis.

HDAC8 is a class I HDAC with a variety of biological functions, such as telomere protection and maintaining the integrity of the acetylation cycle (Romeo et al., 2011). HDAC8 triggers BC cell propagation via Akt/GSK-3β/Snail signaling, which makes the inhibition of HDAC8 a potential therapeutic approach for breast cancer

patients (Dainichi et al., 2018). Our further recovery experiments showed that HDAC8 knockdown could promote the tube formation and migration of HUVECs, and the simultaneous overexpression of LINC01435 could inhibit these processes.

It has been confirmed that YY1 is a key molecular target of antiangiogenic cancer therapy. Inhibition of CXCR4/YY1 impairs VEGF signaling and angiogenesis during the occurrence and development of tumors (de Nigris et al., 2010). However, there are few reports on the mechanism through which YY1 affects diabetic wound healing, and whether it is related to its regulation of the function of vascular endothelial cells remains unclear. The ALGGEN-PROMO website predicted that there was a binding site for the transcription factor YY1 in the promoter region of HDAC8, and we further found that Exos treatment could reduce the expression of HDAC8 by overexpressing LINC01435 and knocking down YY1.

In conclusion, our findings demonstrate an important role of exosomal LINC01435 derived from HaCaT cells in diabetic wound healing. LINC01435 enriched in HG-Exos could enter endothelial cells and increase the expression of HDAC8 by inducing the transport of YY1 into the nucleus, thereby inhibiting the tube formation and migration ability of endothelial cells and ultimately affecting angiogenesis. These results suggest that LINC01435/YY1/HDAC8 may be an important signaling pathway affecting the recovery of diabetic wounds, which makes it a potential target for the treatment of diabetic foot ulcers.

Limitations of the study

This study only investigated the effect of keratinocyte exosome-derived long noncoding RNAs on endothelial cell angiogenesis. The influence of other components of keratinocyte exosomes on endothelial cell function or the biological behavior of other cellular components in the skin microenvironment can be further investigated.

STAR★METHODS

Detailed methods are provided in the online version of this paper and include the following:

- KEY RESOURCES TABLE
- RESOURCE AVAILABILITY
  - Lead contact
  - Materials availability
  - Data and code availability
- EXPERIMENTAL MODEL AND SUBJECT DETAILS
  - For human studies
  - For animal studies
  - For cell lines
- METHOD DETAILS
  - Cell culture
  - Exosome extraction and identification
  - Uptake of the labeled exosomes by endothelial cells
  - Tube formation assay
  - Western blot analysis
  - Proliferation assay
  - Flow cytometric analysis
  - Migration assay
  - RNA purification and qRT–PCR
  - Cell transfection
  - Luciferase reporter assay
  - Chromatin immunoprecipitation (ChIP)
  - LncRNA pull-down assay
  - Animal experiments
- QUANTIFICATION AND STATISTICAL ANALYSIS

SUPPLEMENTAL INFORMATION

Supplemental information can be found online at https://doi.org/10.1016/j.isci.2022.104006.

ACKNOWLEDGMENTS

We thank Wei Wang, Liangyan Wu, and Xiaodan He for the helpful discussion. This work is supported by grants from the National Natural Science Foundation of China: No. 81870571 and U20A20352; Guangdong Basic and Applied Basic Research Foundation: No. 2021B1515020005; Guangdong Science and Technology Department: No. 2020B1212060018 and 2020B1212030004.

AUTHOR CONTRIBUTIONS

W.F., D.F.L., X.Y.W., H.X.C., X.S.H., J.H.W., T.X.Z., T.T.Z., W.J.L., S.F.C., L.Y., and M.R. researched data. D.F.L., H.X.C., X.S.H., J.H.W., T.X.Z., and T.T.Z. analyzed and interpreted the data. W.F. and M.R. designed the study. W.J.L., S.F.C., L.Y., and M.R. contributed to the discussion and reviewed and edited the manuscript. W.F. and X.Y.W. wrote the manuscript. All authors approved the manuscript. W.F. is the guarantor of this work, and as such, had full access to all the data in the study and takes responsibility for the integrity of the data and the accuracy of the data analysis.

DECLARATION OF INTEREST

The authors declare no competing interests.

INCLUSION AND DIVERSITY

We worked to ensure sex balance in the selection of non-human subjects. We worked to ensure diversity in experimental samples through the selection of the cell lines. We worked to ensure diversity in experimental samples through the selection of the genomic datasets. The author list of this paper includes contributors from the location where the research was conducted who participated in the data collection, design, analysis, and/or interpretation of the work.

Received: October 25, 2021
Revised: December 22, 2021
Accepted: February 25, 2022
Published: April 15, 2022

REFERENCES

An, P., Chen, F., Li, Z., Ling, Y., Peng, Y., Zhang, H., Li, J., Chen, Z., and Wang, H. (2020). HDAC8 promotes the dissemination of breast cancer cells via AKT/GSK-3beta/Snail signals. Oncogene *39*, 4956–4969.

Bakker, K., Apelqvist, J., Lipsky, B.A., and Van Netten, J.J.; International Working Group on the Diabetic, F (2016). The 2015 IWGDF guidance documents on prevention and management of foot problems in diabetes: development of an evidence-based global consensus. Diabetes Metab. Res. Rev. *32* (*Suppl 1*), 2–6.

Bao, M.H., Li, G.Y., Huang, X.S., Tang, L., Dong, L.P., and Li, J.M. (2018). Long noncoding RNA LINC00657 acting as a miR-590-3p sponge to facilitate low concentration oxidized low-density lipoprotein-induced angiogenesis. Mol. Pharmacol. *93*, 368–375.

Cech, T.R., and Steitz, J.A. (2014). The noncoding RNA revolution-trashing old rules to forge new ones. Cell *157*, 77–94.

Dainichi, T., Kitoh, A., Otsuka, A., Nakajima, S., Nomura, T., Kaplan, D.H., and Kabashima, K. (2018). The epithelial immune microenvironment (EIME) in atopic dermatitis and psoriasis. Nat. Immunol. *19*, 1286–1298.

de Nigris, F., Crudele, V., Giovane, A., Casamassimi, A., Giordano, A., Garban, H.J., Cacciatore, F., Pentimalli, F., Marquez-Garban, D.C., Petrillo, A., et al. (2010). CXCR4/YY1 inhibition impairs VEGF network and angiogenesis during malignancy. Proc. Natl. Acad. Sci. U S A *107*, 14484–14489.

Deardorff, M.A., Bando, M., Nakato, R., Watrin, E., Itoh, T., Minamino, M., Saitoh, K., Komata, M., Katou, Y., Clark, D., et al. (2012). HDAC8 mutations in Cornelia de Lange syndrome affect the cohesin acetylation cycle. Nature *489*, 313–317.

DeFronzo, R.A., Ferrannini, E., Groop, L., Henry, R.R., Herman, W.H., Holst, J.J., Hu, F.B., Kahn, C.R., Raz, I., Shulman, G.I., et al. (2015). Type 2 diabetes mellitus. Nat. Rev. Dis. Primers *1*, 15019.

Emmons, M.F., Faiao-Flores, F., Sharma, R., Thapa, R., Messina, J.L., Becker, J.C., Schadendorf, D., Seto, E., Sondak, V.K., Koomen, J.M., et al. (2019). HDAC8 regulates a stress response pathway in melanoma to mediate escape from BRAF inhibitor therapy. Cancer Res. *79*, 2947–2961.

Falanga, V. (2005). Wound healing and its impairment in the diabetic foot. Lancet *366*, 1736–1743.

Galkowska, H., Wojewodzka, U., and Olszewski, W.L. (2006). Chemokines, cytokines, and growth factors in keratinocytes and dermal endothelial cells in the margin of chronic diabetic foot ulcers. Wound Repair Regen. *14*, 558–565.

Guttman, M., Russell, P., Ingolia, N.T., Weissman, J.S., and Lander, E.S. (2013). Ribosome profiling provides evidence that large noncoding RNAs do not encode proteins. Cell *154*, 240–251.

Ho, R.X., Meyer, R.D., Chandler, K.B., Ersoy, E., Park, M., Bondzie, P.A., Rahimi, N., Xu, H., Costello, C.E., and Rahimi, N. (2018). MINAR1 is a Notch2-binding protein that inhibits angiogenesis and breast cancer growth. J. Mol. Cell Biol. *10*, 195–204.

Hu, Y., Rao, S.S., Wang, Z.X., Cao, J., Tan, Y.J., Luo, J., Li, H.M., Zhang, W.S., Chen, C.Y., and Xie, H. (2018). Exosomes from human umbilical cord blood accelerate cutaneous wound healing through miR-21-3p-mediated promotion of angiogenesis and fibroblast function. Theranostics *8*, 169–184.

Huarte, M., Guttman, M., Feldser, D., Garber, M., Koziol, M.J., Kenzelmann-Broz, D., Khalil, A.M., Zuk, O., Amit, I., Rabani, M., et al. (2010). A large intergenic noncoding RNA induced by p53 mediates global gene repression in the p53 response. Cell *142*, 409–419.

Lee, K.B., Choi, J., Cho, S.B., Chung, J.Y., Moon, E.S., Kim, N.S., and Han, H.J. (2011). Topical embryonic stem cells enhance wound healing in diabetic rats. J. Orthop. Res. *29*, 1554–1562.

Li, B., Luan, S., Chen, J., Zhou, Y., Wang, T., Li, Z., Fu, Y., Zhai, A., and Bi, C. (2020). The MSC-

derived exosomal lncRNA H19 promotes wound healing in diabetic foot ulcers by upregulating PTEN via MicroRNA-152-3p. Mol. Ther. Nucleic Acids *19*, 814–826.

Lim, R., Sugino, T., Nolte, H., Andrade, J., Zimmermann, B., Shi, C., Doddaballapur, A., Ong, Y.T., Wilhelm, K., Fasse, J.W.D., et al. (2019). Deubiquitinase USP10 regulates Notch signaling in the endothelium. Science *364*, 188–193.

Limbourg, F.P., Takeshita, K., Radtke, F., Bronson, R.T., Chin, M.T., and Liao, J.K. (2005). Essential role of endothelial Notch1 in angiogenesis. Circulation *111*, 1826–1832.

Lindner, V., Booth, C., Prudovsky, I., Small, D., Maciag, T., and Liaw, L. (2001). Members of the Jagged/Notch gene families are expressed in injured arteries and regulate cell phenotype via alterations in cell matrix and cell-cell interaction. Am. J. Pathol. *159*, 875–883.

Mobley, R.J., Raghu, D., Duke, L.D., Abell-Hart, K., Zawistowski, J.S., Lutz, K., Gomez, S.M., Roy, S., Homayouni, R., Johnson, G.L., et al. (2017). MAP3K4 controls the chromatin modifier HDAC6 during trophoblast stem cell epithelial-to-mesenchymal transition. Cell Rep. *18*, 2387–2400.

Pefanis, E., Wang, J., Rothschild, G., Lim, J., Kazadi, D., Sun, J., Federation, A., Chao, J., Elliott, O., Liu, Z.P., et al. (2015). RNA exosome-regulated long non-coding RNA transcription controls super-enhancer activity. Cell *161*, 774–789.

Rinn, J.L., and Chang, H.Y. (2012). Genome regulation by long noncoding RNAs. Annu. Rev. Biochem. *81*, 145–166.

Romeo, F., Falbo, L., Di Sanzo, M., Misaggi, R., Faniello, M.C., Barni, T., Cuda, G., Viglietto, G., Santoro, C., Quaresima, B., et al. (2011). Negative transcriptional regulation of the human periostin gene by YingYang-1 transcription factor. Gene *487*, 129–134.

Shabbir, A., Cox, A., Rodriguez-Menocal, L., Salgado, M., and Van Badiavas, E. (2015). Mesenchymal stem cell exosomes induce proliferation and migration of normal and chronic wound fibroblasts, and enhance angiogenesis in vitro. Stem Cells Dev. *24*, 1635–1647.

Shi, Y., Seto, E., Chang, L.S., and Shenk, T. (1991). Transcriptional repression by YY1, a human GLI-Kruppel-related protein, and relief of repression by adenovirus E1A protein. Cell *67*, 377–388.

Skotland, T., Sagini, K., Sandvig, K., and Llorente, A. (2020). An emerging focus on lipids in extracellular vesicles. Adv. Drug Deliv. Rev. *159*, 308–321.

Tsai, M.J., Hsu, Y.L., and Kuo, P.L. (2018). Circulating extracellular vesicles in human disease. N. Engl. J. Med. *379*, 2179–2180.

Xu, Y., Ouyang, L., He, L., Qu, Y., Han, Y., and Duan, D. (2020). Inhibition of exosomal miR-24-3p in diabetes restores angiogenesis and facilitates wound repair via targeting PIK3R3. J. Cell Mol. Med. *24*, 13789–13803.

Yu, M., Liu, W., Li, J., Lu, J., Lu, H., Jia, W., and Liu, F. (2020). Exosomes derived from atorvastatin-pretreated MSC accelerate diabetic wound repair by enhancing angiogenesis via AKT/eNOS pathway. Stem Cell Res. Ther. *11*, 350.

Zhang, J., Chen, C., Hu, B., Niu, X., Liu, X., Zhang, G., Zhang, C., Li, Q., and Wang, Y. (2016). Exosomes derived from human endothelial progenitor cells accelerate cutaneous wound healing by promoting angiogenesis through Erk1/2 signaling. Int. J. Biol. Sci. *12*, 1472–1487.

Zhao, J., Liu, C., Li, Y., Ma, Y., Deng, J., Li, L., and Sun, J. (2020). Thermophoretic detection of exosomal microRNAs by nanoflares. J. Am. Chem. Soc. *142*, 4996–5001.

Zhou, Y., Huan, L., Wu, Y., Bao, C., Chen, B., Wang, L., Huang, S., Liang, L., and He, X. (2020). LncRNA ID2-AS1 suppresses tumor metastasis by activating the HDAC8/ID2 pathway in hepatocellular carcinoma. Cancer Lett. *469*, 399–409.

STAR★METHODS

KEY RESOURCES TABLE

REAGENT or RESOURCE	SOURCE	IDENTIFIER
Antibodies		
CD9	Abcam	ab92726
TSG101	Abcam	ab125011
Grp94	Abcam	ab108606
HDAC8	CST	66042S
YY1	Proteintech	66281
Bacterial and virus strains		
pGL3-basic-HDAC8	Dahong	PR213116
pcDNA3.1(+)-Flag-YY1	Jingbai	PPL00870-2c
pCMV-HA-HDAC8	Dahong	OENM_018486
PRL-TK	Dahong	PR2011092
pGL3-basic	Dahong	PR2011091
Biological samples		
Skin tissue from non-diabetic patients	Sun Yat-sen Memorial Hospital affiliated sun Yat-sen University	N/A
Skin tissue from the feet of diabetic patients	Sun Yat-sen Memorial Hospital affiliated sun Yat-sen University	N/A
Great saphenous vein tissue in a non-diabetic patient	Sun Yat-sen Memorial Hospital affiliated sun Yat-sen University	N/A
Great saphenous vein tissue in a diabetic patient	Sun Yat-sen Memorial Hospital affiliated sun Yat-sen University	N/A
Chemicals, peptides, and recombinant proteins		
Lipofectamine 3000	Thermo Fisher Scientific	L3000-015
Critical commercial assays		
EdU-555	EpiZyme	CX003
Cell Counting Kit-8 (CCK-8)	APExBIO	K1018
Annexin V-FITC/PI	CWBIO	CW2574S
PKH26	Sigma–Aldrich	MINI26
Deposited data		
Original western blot images, high-throughput sequencing and proteomics data.	Mendeley	https://doi.org/10.17632/t5dh6hsm72.1
Experimental models: Cell lines		
HaCaT	Cell Biological	CL-0090
HUVECs	Cell Biological	FH1122
Experimental models: Organisms/strains		
Bks-db	Gempharmatech-GD	T002407-1
Bks-db-WT	Gempharmatech-GD	T002407-2
Oligonucleotides		
SI-NC	RiboBio	siQ0001
SI-HDAC8	RiboBio	P202012180038

(*Continued on next page*)

Continued

REAGENT or RESOURCE	SOURCE	IDENTIFIER
SI-YY1	RiboBio	P202012070066
SM-NC	RiboBio	P202008150001
SM-LINC01435	RiboBio	P202008150001
Recombinant DNA		
pGL3-basic-HDAC8	Dahong	PR213116
pCMV-HA-HDAC8	Dahong	OENM_018486
PRL-TK	Dahong	PR2011092
pGL3-basic	Dahong	PR2011091
pGL3-basic-HDAC8-Mut	This paper	N/A
pcDNA3.1(+)-Flag-YY1	Jingbai	PPL00870-2c
Software and algorithms		
ImageJ	National Institutes of Health	https://imagej.nih.gov/ij/
GraphPad Prism 5	GraphPad Software	https://www.graphpad.com/

RESOURCE AVAILABILITY

Lead contact

Further information and requests for resources and reagents should be directed to and will be fulfilled by the lead contact, Meng Ren (renmeng80@139.com).

Materials availability

This study did not generate new unique reagents.

Data and code availability

Original western blot images, high-throughput sequencing and proteomics data have been deposited at Mendeley and are publicly available as of the date of publication. The DOI is listed in the key resources table. Microscopy data reported in this paper will be shared by the lead contact upon request. Any additional information required to reanalyze the data reported in this paper is available from the lead contact upon request.

EXPERIMENTAL MODEL AND SUBJECT DETAILS

For human studies

Great saphenous vein tissue of 6 diabetic and 4 healthy controls were collected at the Sun Yat-Sen Memorial Hospital (Guangzhou, China) from December 2017 to December 2019. Informed consent was signed by all patients who participated in the study. The Institutional Review Committee of Sun Yat-sen Memorial Hospital, Sun Yat-sen University, Guangdong Province, China, approved the research protocol, which was in line with the principles of the second edition of the Helsinki Declaration.

For animal studies

Wild-type and db/db diabetic 7-week-old male mice were purchased from Guangzhou Yaokang Animal Center (Cat# T002407-1 and T002407-2). All mice were housed under a 12 h light/dark cycle at constant temperature (20°C). The Sun Yat-sen University Animal Protection and Use Committee approved all animal protocols.

For cell lines

HaCaT cells were obtained from ProCell (Cat#CL-0090, Cell Biological Biotechnology Co. LTD, Guangzhou, China) and endothelial cells were also purchased from ProCell (Cat#FH1122, Cell Biological Biotechnology Co. LTD).

METHOD DETAILS

Cell culture

HaCaT cells were obtained from ProCell (Cat#CL-0090, Cell Biological Biotechnology Co. LTD, Guangzhou, China) and cultured in Minimum Essential Medium (MEM, Procell, Wuhan, China) containing 10% fetal bovine serum (FBS, Gibco, Thermo Fisher Scientific, New York, USA). Endothelial cells were purchased from ProCell (Cat#FH1122, Cell Biological Biotechnology Co. LTD) and cultured in endothelial cell medium (ECM, ScienCell, San Diego, California) containing 5% FBS. All cells were cultured in a humid atmosphere with 5% CO_2 at a temperature of 37°C. Mycoplasma contamination was excluded in all cell lines using a commercial kit (Genecreate Biological engineering Co., Ltd, Wuhan, China). We used the normal sugar (5.5 mmol/L) treatment group as the control and balanced the osmotic pressure with mannitol (22.7 mmol/L), labeled NG. High glucose (33.3 mmol/L) group was labeled as HG.

Exosome extraction and identification

When the HaCaT cells reached 50% confluence, exosome-free serum was used for culture, and normal glucose (5.5 mmol/L) and high glucose (33.3 mmol/L) aliquots were added to the MEM medium (Procell) of the control group and treatment group, respectively. After 48 hours of culture, the collected cell supernatant was centrifuged to remove cell debris (300 × g for 10 min, 3000 × g for 20 min), and the supernatant was filtered through a 0.22-μm pore-size membrane (Guangzhou Jet Bio-Filtration Co., Ltd) for subsequent experiments. Then, the supernatant was centrifuged at 10000 × g for 30 min and transferred to a new ultrafiltration tube. This supernatant was centrifuged at 110000 × g for 70 min, and the pellet was resuspended in PBS (Guangzhou Jet Bio-Filtration Co., Ltd) after the resulting supernatant was removed. After repeated centrifugation at 110000 × g for 70 min, the supernatant was removed, and the pellet was resuspended in an appropriate amount of PBS for subsequent exosome characterization. All operations were carried out at 4°C. The expression of the CD9 (1:1000; Abcam, UK), TSG101 (1:1000; Abcam) and Grp94 (1:1000; Abcam) protein markers was detected by western blotting to confirm the exosome isolations were successful.

Uptake of the labeled exosomes by endothelial cells

Exosomes were labeled with red fluorescent dye (PKH26; Sigma–Aldrich, Merck KGaA, Darmstadt, Germany) according to the manufacturer's instructions. Briefly, 2 × 106 cell-derived exosomes were suspended in 100 μL PBS, and 4 μL 1:250 diluted PKH26 (diluted with diluent C) was added. After incubation at room temperature for 5 min, an equal volume of exosome-free serum was added to stop the reaction. The labeled exosomes were collected, washed twice with PBS, and finally resuspended in PBS. The labeled exosomes were added to the endothelial cells and incubated at 37°C for 24 h. After washing the cells three times with PBS, the cells were fixed with 4% paraformaldehyde for 15 min. Then, the formaldehyde was discarded, and the fixed cells were rinsed with PBS three times, followed by the addition of 4,6-diamino-2-phenylindole (DAPI, Biyuntian Biotechnology Co., Ltd., Shanghai, China) to counterstain the nuclei for 5 minutes. After rinsing with PBS three times, an appropriate amount of anti-fluorescence quenching reagent was added, and the stained cells were observed under a confocal laser scanning microscope (LSM 800 with Airyscan, Zeiss, Germany). All operations were carried out in the dark.

Tube formation assay

Angiogenic slides (Ibidi, Germany) were used to measure the angiogenic capacity of endothelial cells *in vitro*. Matrigel (BD, Franklin Lakes, NJ, USA) was thawed at 4°C the day before the tube-formation experiment. Before the experiment, 10 μL Matrigel was added to angiogenic glass slides, and the slides were incubated for 30 min at 37°C. Twelve thousand cells in 50 μL serum-free ECM were placed into the upper compartment. Photographs were taken after the cells were incubated for 12–16 hours. The vascular endothelial cell tube formation was observed using an automated fluorescence microscope (Olympus IX83). The experiments were performed in triplicate.

Western blot analysis

Protein samples were prepared using radioimmunoprecipitation analysis (RIPA) lysis buffer (CWBIO, Beijing, China) with the addition of protease and phosphatase inhibitors (CWBIO). Total protein levels in cells and exosomes were measured using the BCA Protein Assay Kit (Thermo Fisher Scientific). Western blotting was performed with equal amounts of protein (10 or 20 μg). Protein extracts were separated by 10% sodium dodecyl sulfate polyacrylamide gel electrophoresis (SDS–PAGE, Boster Biological Technology

Co., Ltd., California, USA) and then transferred to a polyvinylidene fluoride (PVDF) membrane (Merck-Millipore, Darmstadt, Germany). The PVDF membrane was incubated with antibodies against GAPDH (1:10000; Servicebio, Wuhan, China), HDAC8 (1:1000; CST, Danvers, MA, USA) and YY1 (1:1000; Proteintech, Sanying Biotechnology Co., LTD, Wuhan, China) at 4°C overnight. The cells were incubated with horseradish peroxidase-conjugated secondary antibody for 1 h at room temperature. After rinsing 3 times, the protein bands were developed using ECL reagent (Thermo Fisher Scientific) and recorded using a Mini Chemi imaging system (Sagecreation). The band strength was quantified using ImageJ 5.0 software, and the relative expression levels of HDAC8 and YY1 were normalized to GAPDH.

Proliferation assay

Cell proliferation was assessed using the cell counting kit 8 (CCK-8) assay (CWBiotech, Beijing, China) according to the manufacturer's instructions. 5-Ethyl-2-deoxyuridine (EdU, EpiZyme Biological Medicine Technology Co., LTD, Shanghai, China) DNA proliferation analysis was performed according to the manufacturer's instructions using images obtained at 100x magnification using an inverted fluorescence microscope. The percentage of EdU-positive cells was calculated based on 6 random visual fields using ImageJ software.

Flow cytometric analysis

Endothelial cells from different treatment groups were collected, washed once with PBS and resuspended in 100 μL of binding buffer. Annexin V-FITC (Elabscience Biotechnology Co., LTD, Wuhan, China) (5 μL) and propidium iodine (PI) reagent (10 μL) were added, and the cells were incubated at room temperature in the dark for 15 min. Finally, a FACS instrument (Becton Dickinson, Franklin Lakes, NJ, USA) was used to quantify the fluorescent cells. The experiment was repeated three times with three pairs of wells in each round.

Migration assay

Transwell chambers (24 wells, 8 mm aperture, Corning CoStar, Cambridge, MA, USA) were used to detect the migration ability of endothelial cells *in vitro*. The lower chamber was filled with 650 μL ECM medium containing 5% FBS, and 24,000 cells in 100 μL serum-free ECM were placed into the upper chamber. After incubation for 16–20 hours, the cells were fixed with 0.4% paraformaldehyde and stained with 0.1% crystal violet. Image-Pro Plus (IPP) v6.0 software (Media Cybernetics Inc., Rockville, MD, USA) was used to count the migrating cells. The experiments were performed in triplicate.

RNA purification and qRT–PCR

Total RNA was extracted using TRIzol reagent (Invitrogen, Carlsbad, CA, USA) according to the manufacturer's instructions. The first strand of mRNA was reverse-transcribed with 2 μg total RNA using the FastKing gDNA Dispelling RT SuperMix Kit, and real-time quantitative polymerase chain reaction was performed using the Super Real Premix Plus Kit (SYBR Green, Tiangen, Beijing, China). TB Green™ Premix ExtaQTM II was used for qRT–PCR analysis on a LightCycler 480 II instrument (Roche, Merck). GAPDH was used as an internal reference for lncRNAs and other target genes, and the relative level of gene expression was calculated using the $2^{-\Delta\Delta CT}$ method. All primer sequences are listed in Tables S1 and S2.

Cell transfection

HUVECs were cultured in six-well plates and transfected with a LINC01435 smart silence (SM-LINC01435) or negative control (SM-NC) (RiboBio, Guangzhou, China) at a final concentration of 100 nM using Lipofectamine 3000 (Thermo Fisher Scientific) according to the manufacturer's instructions. HUVECs were transfected with YY1 and HDAC8 siRNA or NC (RiboBio) at a final concentration of 50 nM. The CDSs of YY1 and HDAC8 were cloned into the pcDNA3.1 plasmid (Dahong Biotechnology Co., Ltd., Guangzhou, China) and transfected into HUVECs to upregulate YY1 and HDAC8 expression.

Luciferase reporter assay

The online databases UCSC, ALGGEN PROMO and JASPAR were used to predict the promoter region of HDAC8, the binding site of transcription factor YY1 and the possible binding sequence, respectively. The promoter sequence of HDAC8 was chemically synthesized and cloned into the pGL3-basic vector (Dahong Biotechnology Co., Ltd.) between the *KpnI*/*Bgl*II sites. Lipofectamine 3000 (Invitrogen) was used to

transfect the indicated cells with pGL3-basic-HDAC8 (wild type and mutant), PRL-TK, LINC01435 and si-YY1, and the relative luciferase activity was measured 36 h after transfection using a dual luciferase assay kit (Promega, Beijing, China).

Chromatin immunoprecipitation (ChIP)

Approximately 4 × 10^6 cells were collected for each ChIP reaction. Cross-linked cells were collected according to the instructions, and ChIP lysate was added for ultrasonic treatment to fragment the chromatin. Then, 50 μL of the solution containing cross-linked chromatin fragments was purified using a ChIP kit (Cell Signaling Technology), and 10 μL of the resulting purified DNA was subjected to 1% agarose gel electrophoresis to observe the size of the DNA fragments. The cell lysates of different treatment groups were combined with YY1 (Proteintech) and IgG (negative control; Abcam) for the ChIP assay, and the bound DNA was purified for quantitative analysis by qPCR. TB Green™ Premix ExtaQTM II was used to perform qRT–PCR analysis on a LightCycler 480 II instrument (Roche), and the ChIP-enrichment rate was calculated according to the experimental results.

LncRNA pull-down assay

Streptavidin magnetic beads (MedChemExpress, Haoyuan Biological Medicine Technology Co., LTD, Shanghai, China) were washed with 0.1 M NaOH and 50 nM NaCl solution twice and then once more with the same volume of 100 mM NaCl. The beads were then resuspended in an equal volume of RNA capture buffer, rinsed twice with an equal volume of 20 mM Tris, followed by the addition of 400 pmol of LINC01435 or control probe, and incubated for 2 hours at room temperature. After absorption, the supernatant was discarded, and the beads were rinsed twice with an equal volume of 20 mM Tris, followed by the addition of 100 μL 1 × protein-RNA-binding buffer. After absorption, the supernatant was discarded, and 100 μL Master Mix was added to resuspend the magnetic beads, which were rotated overnight at 4°C. Finally, the beads were rinsed 6–8 times with wash buffer and eluted with 50 μL elution buffer at 37°C for 30 minutes. The supernatant was stored at −80°C for further experiments.

Animal experiments

All procedures involving animals in this study were approved by the Animal Research Committee of Sun Yat-sen University. Wild-type and db/db diabetic 7-week-old male mice were purchased from Guangzhou Yaokang Animal Center. After acclimatization for two weeks at the Animal Experimental Center of the East Campus of Sun Yat-Sen University, skin wound modeling was performed. After shaving, a round piece of full-thickness skin tissue with a diameter of 6 mm was cut out from the back of the mice. Wild-type and db/db diabetic mice were randomly divided into 3 groups, two of which were subcutaneously injected with either NG-Exos or HG-Exos (100 μg dissolved in 100 μL PBS) at 4 injection sites and a control group (25 μL PBS at each site). The gross morphology of the wounds of 6 groups of mice was photographed at 0 days, 3 days, 6 days, 9 days and 11 days after the trauma. Skin samples were collected for further IHC and IF experiments after sacrificing the animals 11 days after the surgery.

QUANTIFICATION AND STATISTICAL ANALYSIS

For quantitative analysis, each experiment was carried out at least 3 times, and all values were expressed as the means ± standard deviations (SD) or SEM. GraphPad Prism Software (GraphPad Inc., La Jolla, CA, USA) was used for all data processing and analysis. Two-tailed Student's *t* test was used for comparisons between two groups. Comparisons between results from different groups were performed using one-way ANOVA with Dunnett's T3 multiple comparison analysis. Differences with $p < 0.05$ were considered statistically significant. *$p < 0.05$; **$p < 0.01$; ***$p < 0.001$; ns: no significance.